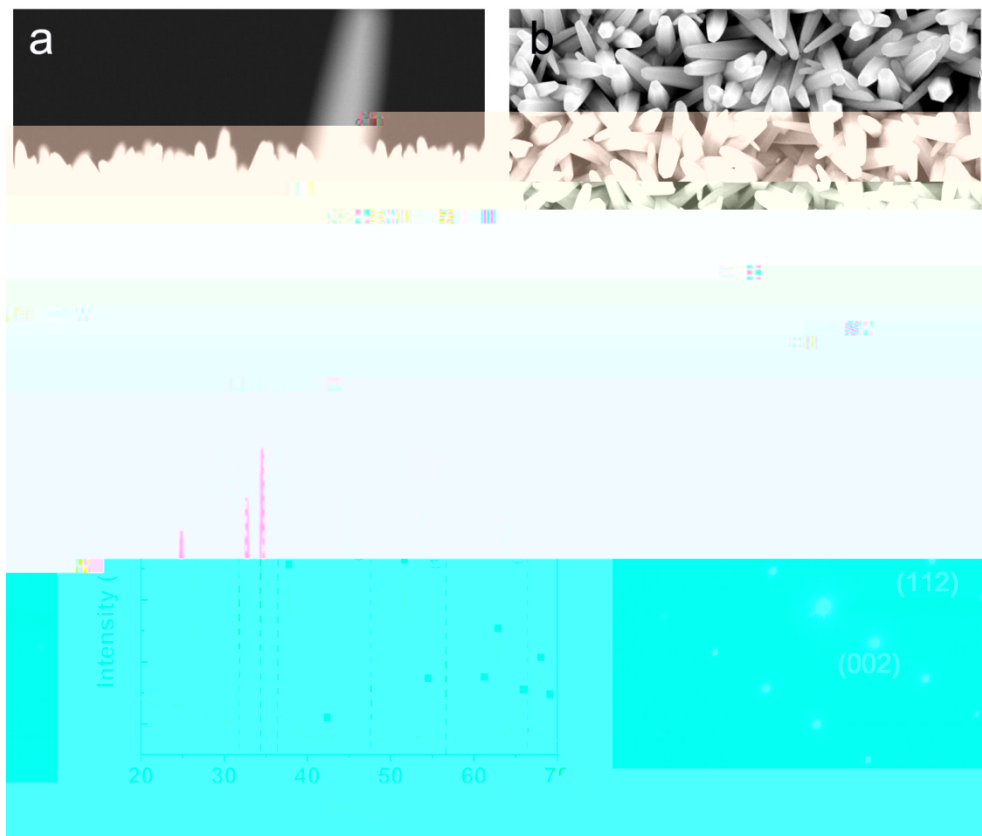


Zhongqiu Tong, Shikun Liu, Xingang Li, Liqiang Mai, Jiupeng Zhao, Yao Li



(a)(b) Cross-sectional and top-view SEM images of the ZnO nanorod arrays. (c) XRD pattern of the ZnO nanorod arrays. (d) SAED pattern of one ZnO nanorod.

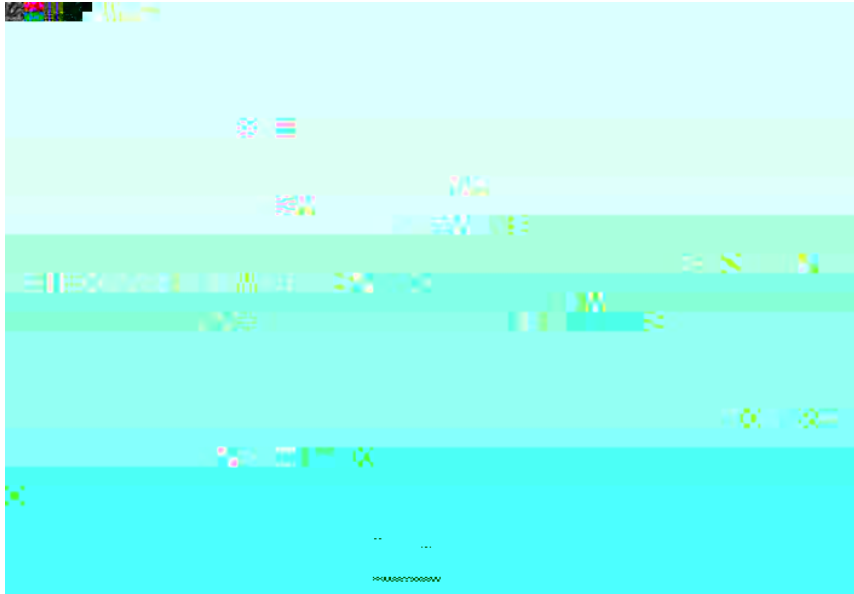


Figure 1. SEM image of large-area ZnO nanorod arrays.

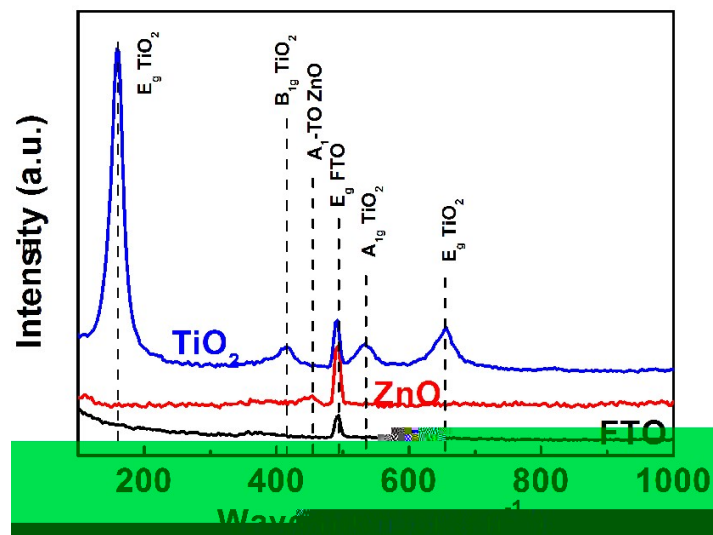


Figure 2. Raman spectra of FTO substrate, ZnO nanorod arrays, and TiO<sub>2</sub> mesoporous nanotube arrays.

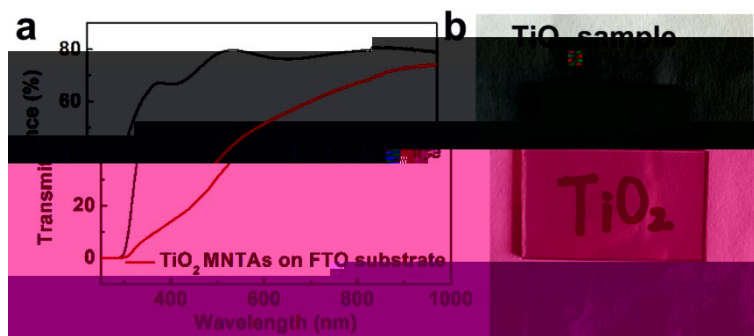


Figure 3. UV-transmission spectra (a) and digital photos (b) of TiO<sub>2</sub> MNTAs and bare FTO substrate.

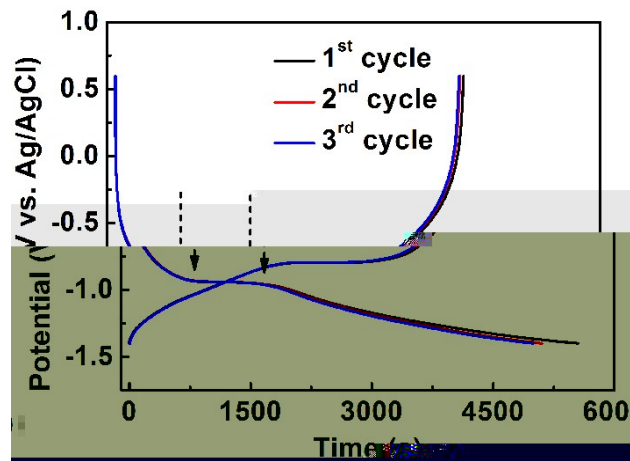


Figure 10. Galvanostatic charge/discharge curves of  $\text{TiO}_2$  MNTAs at 0.75C.

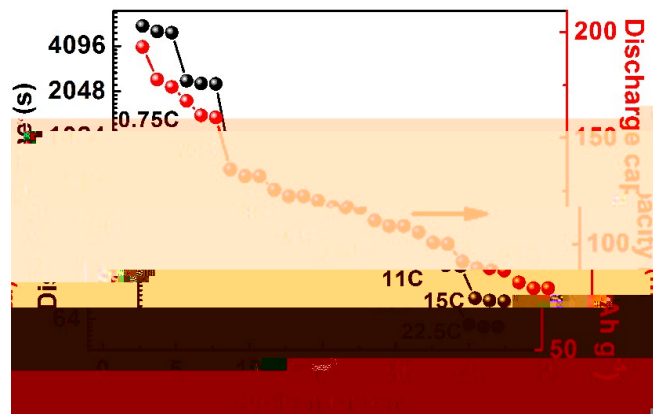


Figure 11. Discharge capacity and discharge time of  $\text{TiO}_2$  MNTAs at different current densities.

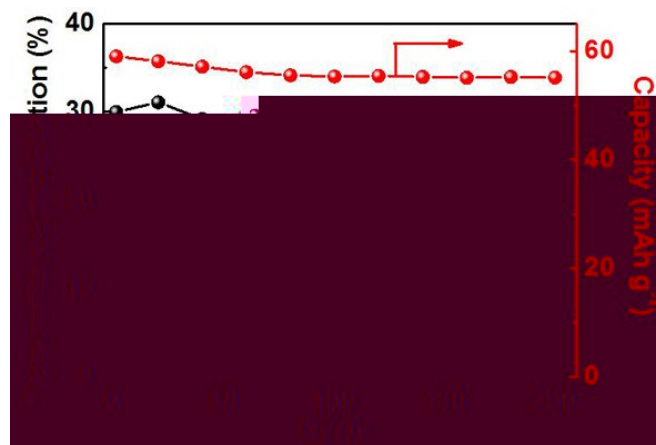


Figure 12. Cycling performance of the assembled bifunctional device on transmittance modulation and capacity at galvanostatic charge/discharge current density of  $1 \text{ A g}^{-1}$ .

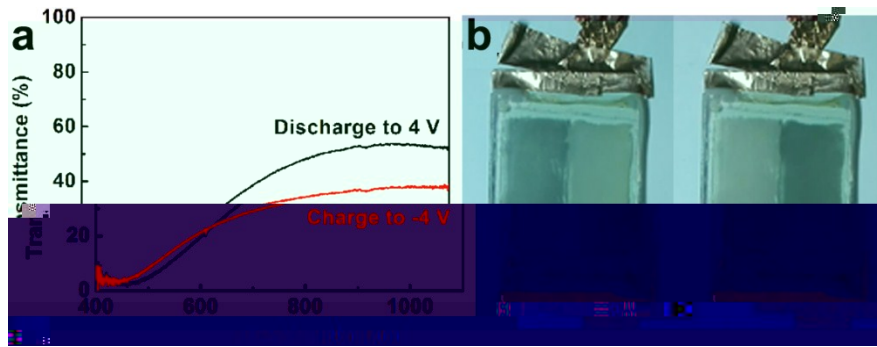


Figure 1. Transmittance modulation (a) and color contrast (b) of the assembled bifunctional device at galvanostatic charge/discharge current density of  $2 \text{ A g}^{-1}$ .